Journal of Solid State Chemistry 186 (2012) 70–75

Contents lists available at SciVerse ScienceDirect

Journal of Solid State Chemistry

journal homepage: www.elsevier.com/locate/jssc

Roles of Bi, *M* and VO_4 tetrahedron in photocatalytic properties of novel $Bi_{0.5}M_{0.5}VO_4$ (*M*=La, Eu, Sm and Y) solid solutions for overall water splitting

Hui Liu [a,b,c], Jian Yuan [b], Zhi Jiang [b], Wenfeng Shangguan [b,*], Hisahiro Einaga [c], Yasutake Teraoka [c,**]

[a] School of Metallurgical Science and Engineering, Central South University, Changsha 410017, PR China
[b] Research Center for Combustion and Environment Technology, Shanghai Jiao Tong University, shanghai 200240, PR China
[c] Faculty of Engineering Sciences, Kyushu University, Fukuoka 816-8580, Japan

ARTICLE INFO

Article history:
Received 17 October 2011
Received in revised form
24 November 2011
Accepted 25 November 2011
Available online 6 December 2011

Keywords:
Rietveld refinement
Bi incorporation
V–O bond
DFT calculation

ABSTRACT

Novel $Bi_{0.5}M_{0.5}VO_4$ (B*M*V; *M*=La, Eu, Sm and Y) solid solutions were prepared and studied in this paper. All the samples were proved to produce H_2 and O_2 simultaneously from pure water under the irradiation of UV light. *M*–O bond lengths were proved to increase with *M* cations by refining cell parameters and atomic positions. Besides, band gaps, energy gaps and photocatalytic activities of BMV also changed with *M* cations. Both of *M*–O and V–O bond lengths were suggested to account for this phenomenon. Inactive $A_{0.5}Y_{0.5}VO_4$ (*A*=La, Ce) for water splitting proved incorporation of Bi rather than distortion of VO_4 tetrahedron was a critical factor for improving efficiency of overall water splitting by facilitating the generation of electron and hole with lighter effective masses. Replacement of Bi by *M* cations not only gave indirect effect on band structure but also raised position of conduction band minimum to meet requirement of H_2 production.

1. Introduction

Hydrogen society is a dream world in which hydrogen is used to replace the oil as a major energy carrier. Since water is the only product when using hydrogen as a fuel, many environmental problems relating to fossil fuels, such as globe warming, acid rain, will be completely solved. However, there is no H_2 deposit on the earth. We have to find a sustainable energy source to convert to hydrogen energy. As we knew, solar energy is one of best energy supplies. In 1972, the significant discovery made by Japanese scientists Fujishima and Honda demonstrated light can be converted to chemical H_2 energy from water by using TiO_2 electrode for the first time [1]. Since then, photoelectrocatalytic (photocatalytic) water splitting has been paid more and more attention to provide the sustainable hydrogen energy from water [2–6] because water and solar energy are two of most abundant resources on the earth.

In general, photocatalytic water splitting can be divided into two types against the photocatalytic properties of catalysts [7]. One is overall water splitting, in which H_2O is decomposed simultaneously into H_2 and O_2 using photocatalyst and light irradiation. In another case, sacrificial reagents are needed to provide electronic donor or electronic scavenger for producing H_2 or O_2, respectively. The photocatalysts used in the second case usually can absorb the visible light and achieve high quantum efficiency. However, the requirement of sacrificial reagents is a limit for providing sustainable H_2 energy. In this sense, overall water splitting is more important than partial water splitting.

To achieve high efficiency for overall water splitting, many factors have been involved in. Roughly those effects can be divided into three types: the first one is bulk properties of catalysts, such as crystal structures [8,9], composition [10,11], particle size [12,13], and so on, which determine semiconducting properties of photocatalysts like photoabsorption properties, electron and hole transport properties. The second one is surface properties including surface crystal structure [14], surface shape [15,16], co-catalyst [2,17] etc. Since surface is where the catalytic reactions take place, these factors have very critical effect on the efficiency. However, the effects of surface properties were still a big challenging to study due to their complexity. The last one is reaction conditions. Many researches have proved that pH [18], electrolyte [19] and even stirring methods [20] play an important role in improving the activity of photocatalysts.

In our previous study, we discovered that a new series photocatalysts of Bi–Y–V oxides, a V-based solid solutions, performed overall water splitting under UV light irradiation with high efficiency [21]. To understand the high efficiency of BYV solid solution for overall water splitting, we successively synthesized other series of $Bi_{0.5}M_{0.5}VO_4$ (B*M*V; *M*=La, Sm, Eu, Y) solid solutions in this paper to investigate the roles of Bi, *M* and VO_4 tetrahedron since we found the photocatalytic activity of B*M*V has

* Corresponding author. Fax: +86 21 34206372.
** Corresponding author. Fax: +81 92 5838853.
E-mail addresses: Shangguan@sjtu.edu.cn (W. Shangguan), Teraoka@mm.kyushu-ac.jp (Y. Teraoka).

0022-4596/$ - see front matter © 2011 Elsevier Inc. All rights reserved.
doi:10.1016/j.jssc.2011.11.035

close relationship with them. Here we just focused on the effect of bulk properties of photocatalysts. The crystal structure and photoabsorption property of B*M*V mixed oxides were characterized. Photocatalytic study proved that $Bi_{0.5}M_{0.5}VO_4$ were stable and highly efficient photocatalysts for overall water splitting as well. The isomorphic compounds $La_{0.5}Y_{0.5}VO_4$ (LYV) and $Ce_{0.5}Y_{0.5}VO_4$ (CYV) were also prepared and investigated to understand the roles of Bi and VO_4 tetrahedron. Band structures of $BiVO_4$, YVO_4 and $Bi_{0.5}Y_{0.5}VO_4$ (BYV) were calculated using WIEN2k in the framework of density function theory. Based on the experimental and computing results of BYV solid solutions, the roles of Bi, *M* and VO_4 in the photocatalytic activity of overall water splitting were discussed and proposed.

2. Experimental section

2.1. Preparation of photocatalysts

B*M*V solid solutions were prepared by solid-state reactions. The starting materials were V_2O_5 (99%, Wako Chemical), M_2O_3 (*M*=La, Eu, Sm and Y; 99.9%, Wako Chemical), and Bi_2O_3 (99.9%, Wako Chemical). M_2O_3 was heated at 873 K for 1 h in air for dehydration before use. Desired proportions were weighted and thoroughly mixed in the presence of ethanol. After ethanol was evaporated, the mixtures were heated at 1073 K in covered ceramic crucibles in air for 24 h with one grinding. LYV and CYV solid solutions were also prepared in the same procedures. CeO_2 (99%, Wako) was used as Ce source. CeO_2 can be reduced to Ce^{3+} at high temperature [22].

To load the co-catalyst, the prepared mixed oxides were added to $Cr(NO_3)_3$ and $Na_3RhCl_6 \cdot 2H_2O$ aqueous solution. The solution was evaporated to dryness on a water bath at 353 K and then calcined at 623 K for 1 h to load 0.275 wt% Rh and 0.4 wt% Cr_2O_3 together (denoted as Rh–Cr_2O_3) according to the Refs. [23, 24].

2.2. Characterization

To measure UV–vis diffuse reflectance spectra (DRS), samples were mixed with α-Al_2O_3 (Wako Chemical) by a weight ratio of 1:9 (sample:α-Al_2O_3). Spectra of the samples were recorded on a UV–vis spectrometer (Shimadzu UV-3100) equipped with an integrating sphere attachment and converted to absorption through the Kubelka–Munk method. Raman spectra were investigated on a Raman spectrometer (Jasco NRS-2100), in which an Ar^+ laser of 514.5 nm was used as an excitation source.

Crystal structure of a catalyst was examined by powder X-ray diffraction (PXRD) measurement using Cu *K*α radiation (Rigaku RINT-2200, 40 kV, 20 mA) at room temperature in the fixed time mode over an angular range of $10^\circ \leq 2\theta \leq 140^\circ$ with 0.02° (2θ) step and a counting time of 1.5–3.0 s and then refined using Rietveld refinement. Free software Fullprof program was used for this process [25]; and a pseudo-Voigt peak-shape function was used as a profile function.

2.3. Photocatalytic reaction for water splitting

Photocatalytic reactions were carried out under the irradiation of a 450 W Hg lamp in a reaction vessel made of Pyrex glass ($\lambda > 300$ nm), which connected to a glass closed gas circulation and evacuation system. The amounts of pure water and catalysts used in the vessel were 400 mL and 0.2 g, respectively. The amounts and types of gases produced were determined by gas chromatography (Shimadzu GC-8A, Ar carrier).

2.4. Band structure calculation

Band structure was calculated using WIEN2k code with full-potential linearized augmented plane-wave method. This is an implementation of a hybrid full-potential (linear) augmented plane-wave plus local orbitals (L/APW+lo) method within density functional theory. The exchange-correlation energy was calculated using generalized gradient approximation (GGA) [26]. The cutoff parameter $R_{mt}K_{max}$ was set to 7.0. A *k*-space integration by a mesh of 10,000 *k* points was used over the first Brillouin zone for zircon type YVO_4 and $BiVO_4$. A supercell structure was created for the calculation of BYV, in which a mesh of 1000 *k* points was used. The atomic electronic configuration were used in our calculations as follows: O: [He] $2s^2 2p^4$, Y: [Kr] $4d^1 5s^2$, Bi: [Xe] $5d^{10} 6s^2 6P^3$, V: [Ar] $3d^3 4s^2$. We adopted 2.27 Bohr for Bi, 2.29 Bohr for Y, 1.70 Bohr for V, and 1.50 Bohr for O, as muffin-tin sphere radii. The self-consistent calculations were considered to converge only when the calculated total energy of the crystal converged to less than 0.1 mRy. The total and partial densities of states (DOS) were obtained by using a modified tetrahedron method of Blöchl et al. [27].

3. Results and discussion

3.1. Crystal structures and Rietveld refinement of $Bi_{0.5}M_{0.5}VO_4$ (BMV; M=Y, La, Sm, Eu)

B*M*V mixed oxides including mixed *M* cations (25% Y+25% La and 25% Y+25% Eu) were prepared by solid state reaction. The PXRD patterns of those samples are presented in Fig. 1. All the samples except for BLV were of single phase. A small amount of impurity labelled by filled diamond was observed in the BLV sample and identified as $LaVO_4$. From Fig. 1, B*M*V solid solutions were determined to be zircon type structure. However, the peaks from the same crystal indices shifted to the right with the decreasing effective ionic radii of *M* cations from La to Y, indicating the contraction of cell parameters of B*M*V solid solutions. In Fig. 2, cell parameters of B*M*V samples took on linear relationships with the effective ionic radii of *M* elements. This change suggested all the *M* cations should randomly occupy the same symmetric position with Bi cation.

LYV and CYV were also prepared for investigating the state of Bi6*s* lone pair in the compounds. Shannon et al. found that ratios of Bi to La radii had a close connection to the state of Bi 6*s* lone pair by carefully comparing the effective ionic radii of Bi and La cations in many different isomorphisms [28]. When Bi is in the

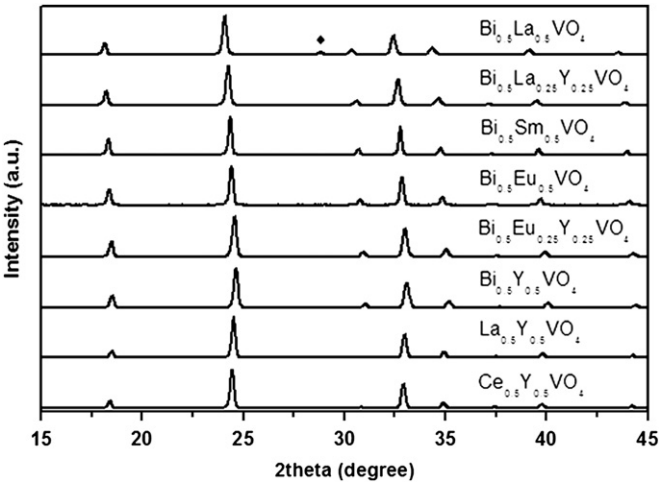

Fig. 1. XRD patterns of B*M*V and $A_{0.5}Y_{0.5}VO_4$ solid solution.

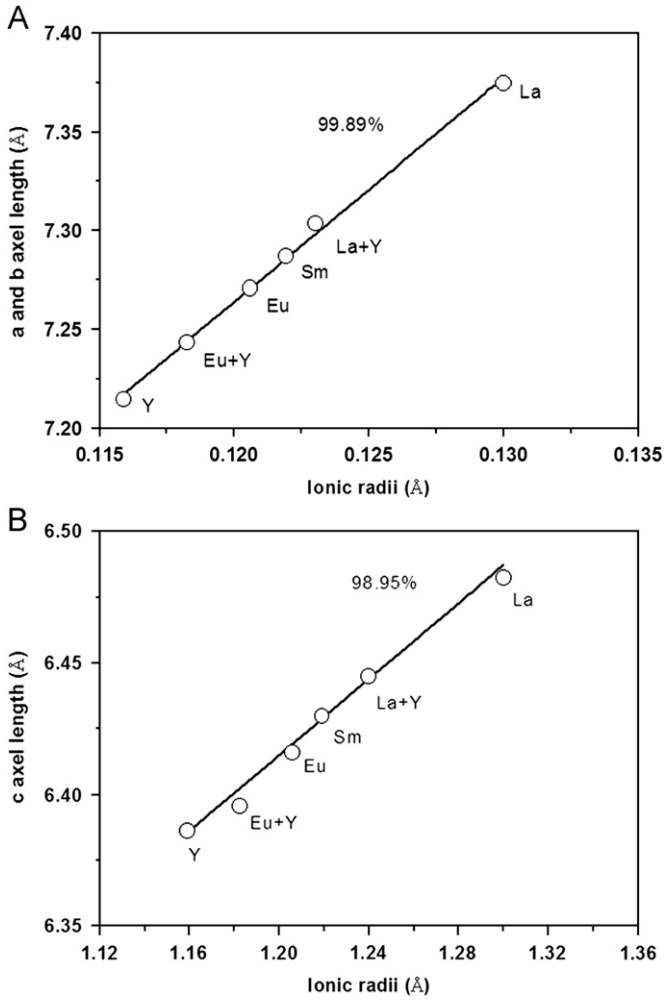

Fig. 2. Cell parameters of B*M*V slid solutions against the effective ionic radii of *M* elements. (A) *a* & *b* axel length and (B) *c* axel length.

Table 1
Cell parameters of $A_{0.5}Y_{0.5}VO_4$ (A=La, Ce, Bi).

	Radii of *A*	*a* & *b*	*c*	*V*
$Bi_{0.5}Y_{0.5}VO_4$	1.092[a]	7.214(6)	6.386(3)	332.4
$La_{0.5}Y_{0.5}VO_4$	1.160[b]	7.274(1)	6.400(0)	338.6
$Ce_{0.5}Y_{0.5}VO_4$	1.143[b]	7.259(7)	6.399(4)	337.3

[a] Estimated value.
[b] Cited from Shannon et al. [21].

constrained state, it has smaller size than La. However, when it equals to or little larger than La, Bi6*s* lone pair turns to the dominant state. As a result, state of Bi6*s* lone pair can be deduced by comparing its effective ionic radii with La. From the data in Fig. 1, LYV and CYV solid solutions also belonged to zircon type structure since they presented the same XRD pattern as BYV with a certain shift. Cell parameters of them as well as BYV were estimated from XRD patterns and listed in Table 1. The effective ionic radius of Bi in BYV solid solution was estimated to be 1.092 Å, rather smaller than 1.16 Å of La in the same crystal structure. According to the above discussion, Bi6*s* lone pair must be in constraint state in BYV solid solution. This evidence proved that Bi6*s* lone pair cannot form a new valence band in BYV solid solution and reduce the band gap as it did in fergusite $BiVO_4$.

To further investigate change of crystal structures of B*M*V solid solutions with *M* cations, Rietveld refinement was used to refine the atomic positions and cell parameters using PXRD data. Zircon type YVO_4 was used as a model structure for atomic position refinement of B*M*V solid solutions. In the zircon type structure, *M* and V cations were fixed at 4a (0, 3/4, 1/8) and 4b (0, 1/4, 3/8) of Wyckoff sites. Only atomic positions of O atom need refinement. The agreement factors and crystal data of zircon-type BMV were listed in Table 2. Since X-ray powder diffraction data were not so accurate for refinement comparing to the neutron diffraction, R_{wp}, R_p and R_{exp} were located in the acceptable range and suggested our refinements were reasonable results.

The *M*–O bond lengths were calculated and presented in Table 2 using the refined atomic positions and cell parameters of B*M*V solid solutions. V–O bond lengths were identical for each sample since VO_4 tetrahedron was usually regarded as a stable structure. They increased slightly with *M* cations from 1.709 Å to 1.716 Å. At the same time, both of Bi(*M*)–O bond lengths in Bi(–)O_8 bisdisphenoids also underwent the same change as V–O bond. In sum, replacement of large radius cations was the reason for elongation of Bi(*M*)–O and V–O bond lengths in B*M*V solid solution.

3.2. Local structure of VO_4 tetrahedron

Besides XRD measurement of crystal structure, we also used Raman spectroscope to investigate the symmetric stretching vibration of VO_4 tetrahedron, which was an indicator to V–O bond length. Six vibration bands were observed for all B*M*V solid solutions as presented in Fig. 3. The strongest peaks were

Table 2
Crystal data and interatomic distances for zircon-type B*M*V solid solutions (M=Y, Eu, Sm, La).

	$Bi_{0.5}Y_{0.5}VO_4$	$Bi_{0.5}Eu_{0.5}VO_4$	$Bi_{0.5}Sm_{0.5}VO_4$	$Bi_{0.5}La_{0.5}VO_4$
R_{wp}	7.79	9.22	8.93	10.44
R_p	11.32	13.33	12.64	14.21
R_{exp}	6.51	8.57	7.34	9.45
G-of-F	1.7	1.9	1.8	2.1
a	7.207(2)	7.262(6)	7.280(5)	7.382(0)
c	6.376(4)	6.411(5)	6.422(2)	6.499(8)
U_{eq}(M)	0.5	0.4	0.4	0.5
y(O)	0.4339	0.4320	0.4318	0.4289
z(O)	0.2050	0.2054	0.2059	0.2076
U_{eq}(O)	0.50	0.68	0.74	0.65
uR(chi^2)	3.02	3.92	3.43	5.41
V–O (Å)	1.709(2)	1.711(0)	1.712(4)	1.716(6)
Bi(*M*)–O (Å)	2.337(1)	2.366(5)	2.374(3)	2.427(3)
Bi(*M*)–O (Å)	2.485(4)	2.497(4)	2.503(1)	2.531(5)

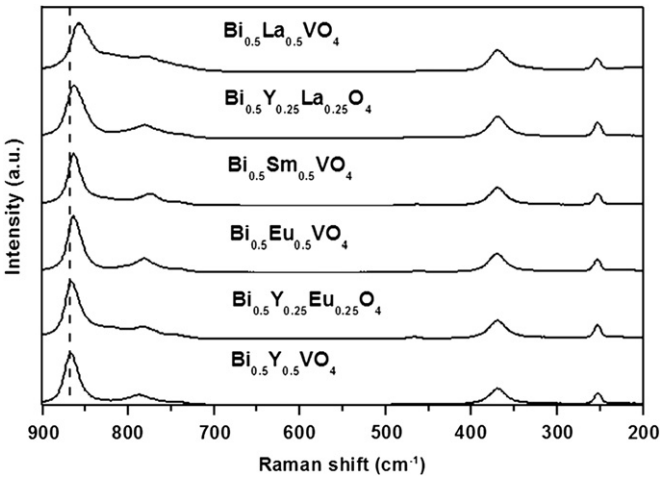

Fig. 3. Raman spectra of B*M*V solid solutions.

assigned to symmetric stretching vibration of VO_4 tetrahedron and shifted from 867 cm^{-1} to 857 cm^{-1} with *M* cations. The movement of symmetric stretching vibration of VO_4 tetrahedron to low frequency meant elongation of V–O bond lengths, which was also observed by Hardcastle et al. [29]. This founding was agreeable with the results from the Rietveld refinement.

Mass effect on Raman modes' frequency was observed in some solid solutions, such as $(X_1, X_2)MoO_4$ and $(X_1, X_2)WO_4$ solid solutions with X_1, X_2 being Sr, Ba, Pb and Ca [30]. The heavier weight of X cations caused the modes' frequency shift to low frequency. But for BMV system, the masses of *M* cations did not exert an influence on Raman modes' frequency since $Bi_{0.5}La_{0.25}Y_{0.25}VO_4$ and $Bi_{0.5}La_{0.5}VO_4$ with lighter mass had the Raman band of lower frequency than $Bi_{0.5}Sm_{0.5}VO_4$ and $Bi_{0.5}Eu_{0.5}VO_4$. Therefore, the different effective ionic radii of *M* and Bi cations were the only reason for the change of VO_4 tetrahedron.

3.3. Photoabsorption properties of BMV solid solutions

The UV–vis DRS of B*M*V solid solutions were shown in Fig. 4. Inflection points of absorption spectrum slope can be observed around 400 nm for all the samples. They indicated there were two kinds of absorption mechanisms for light absorption. The strong and extensive absorption in the high energy zone represented the major transition and can be regarded as band gap. The weak and narrow absorption in the low energy area should originate from the transition of energy level of Bi6*s* since Bi6*s* orbital cannot form band in zircon type structure as we proved in the above section. The band gaps and energy level gaps were estimated and are presented in Table 3 comparing with effective ionic radii of *M* element. Positive relationships between band gaps, energy level gaps and the effective ionic radii of *M* cations were observed. However such relationship had not been observed in other Ln-containing materials like $RbLnTa_2O_7$ [31], $K_2LnTa_5O_{15}$ [32] and Bi_2LnNbO_7 [33]. In those samples, Ln 4*f* bands were suggested to form hybrid band structure and cause visible light absorption. The different contributions of Ln cations indicated changes of the band gaps of B*M*V solid solutions may have no relation with electronic structure of *M* cations. Since both of Bi–O and V–O bond lengths increasing with *M* cations were observed in the above experiments, we suggested *M* cations gave indirect contribution to electron structures of B*M*V solid solution by adjusting the crystal structures of B*M*V solid solution due to the different effective ionic radii of *M* cations.

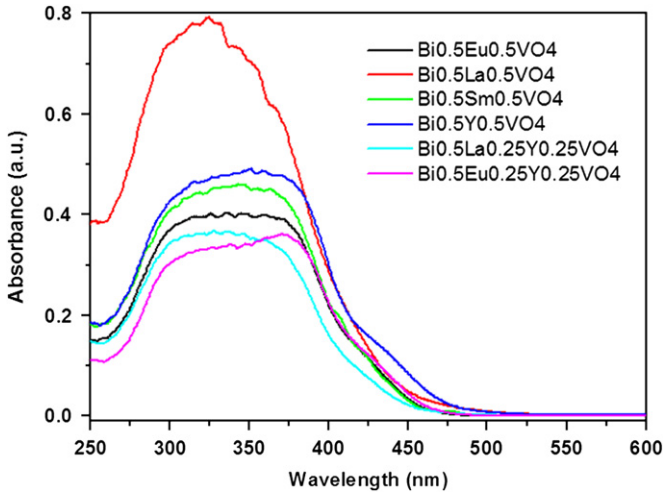

Fig. 4. UV–visible diffuse reflectance spectra of B*M*V solid solutions.

Table 3
Band gaps and energy level gaps of B*M*V solid solutions with effective ionic radii of *M* cations.

M cations	Effective ionic radii/Å	Band gap/eV	Energy gap/eV
La	1.3	3.096	2.672
La/Y	1.23	3.047	2.644
Sm	1.219	3.039	2.65
Eu	1.206	3.017	2.608
Y/Eu	1.183	3.006	2.608
Y	1.159	2.98	2.53

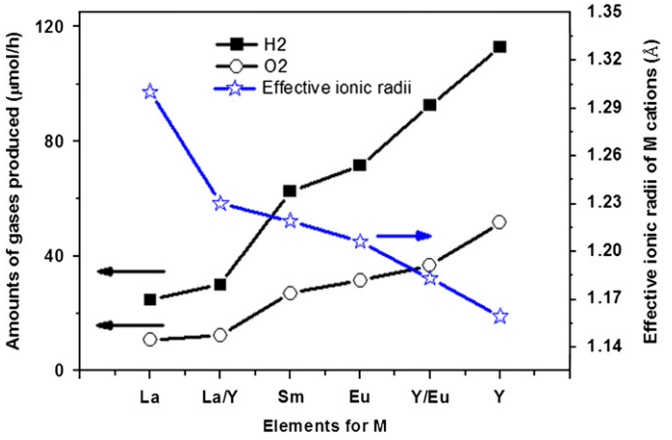

Fig. 5. Photocatalytic activities of B*M*V solid solutions and effective ionic radii of *M* cations.

Based on the above suggestion, band gaps of BMV solid solutions should predominantly come from VO_4 tetrahedron and Bi6*p* orbital. Stuckl and Dolgos [23,24] reported ligand-to-metal charge transfer (LMCT) transition of VO_4 tetrahedron was about 4.3–4.5 eV [34,35] using DFT calculation. When VO_4 tetrahedron formed a condensed matter with other cations, the crystal structures and interactions between the cations and VO_4 narrowed LMCT transition to some extent [34]. Bi6*p* caused a strong interaction with VO_4 tetrahedron and decreased the band gap of $BiVO_4$ to 2.4 eV from 4.3 eV of VO_4 tetrahedron [36–38]. As for BMV solid solutions, incorporation of *M* cations into $BiVO_4$ weakened the interaction between the Bi6*p* and VO_4 tetrahedron by reducing Bi amount and then enhanced the position of conduction band minimum (CBM). When CBM moved over the H_2/H_2O potential with increasing of *M* amounts, it met the electrochemical requirement of water reduction and led to produce H_2. This was considered as a reason why B*M*V solid solutions have the ability to obtain H_2 from water.

3.4. Photocatalytic activity for pure water splitting

All the B*M*V samples were investigated for photocatalytic water splitting under full arc light irradiation ($\lambda > 300$ nm) after loaded 0.275% Rh–0.4% Cr_2O_3 as co-catalysts. 0.2 g samples were used in each experiment. Same to BYV system, all the BMV photocatalysts were also able to split water completely to H_2 and O_2. It was interesting to find that the photocatalytic activity of BMV solid solution had the negative correlation with effective ionic radii of *M* cation as present in Fig. 5. BYV showed the highest production of H_2 and O_2 at 112.7 μmol/h and 51.8 μmol/h, respectively, around 5 times higher than those of $Bi_{0.5}La_{0.5}VO_4$ in the same conditions.

Yu et al. [39] observed that the decreasing V–O bond lengths of $BiVO_4$ enhanced its photocatalytic activity for O_2 production.

This phenomenon is reasonable since Shannon et al. summarized that the electron delocalization of metal–O bond in oxides results in the reduced metal–oxygen distances by comparison of many oxides [28]. Since electron delocalization is a plus factor for photocatalytic activity [40], it is also suitable to use this reason to explain change of photocatalytic activities of B*M*V solid solutions because V–O bond length changed with *M* cations. However, Bi(*M*)–O bond lengths also underwent the same change as V–O bond according to the results of Rietveld refinement. Therefore, we cannot simply ascribe the improved activities only to V–O bond of B*M*V solid solutions.

On the other side, photocatalytic activity of $A_{0.5}Y_{0.5}VO_4$ (*A*=La, Ce, Bi) samples were investigated for water splitting to understand the effect of incorporation of Bi and distortion of VO_4. Results of photocatalytic experiments under UV light irradiation are presented in Table 4. BYV has the high photocatalytic activity for over water splitting as studied in the previous study. However, LYV and CYV performed very weak photocatalytic activities. In 8 h experiment, only about 1 μmol H_2 were produced by two samples. No oxygen was detected due to the small amount which could be dissolved in the water or absorbed on the catalyst [41]. This result proved that Bi cation in B*M*V played an important role in obtaining high efficiency for overall water splitting. On the other hand, distortion of VO_4 tetrahedron has been reported to improve the activity of $BiVO_4$ as presented [34,39]. As concerned as $A_{0.5}Y_{0.5}VO_4$, certain local distortion of VO_4 in $La_{0.5}Y_{0.5}VO_4$ and $Ce_{0.5}Y_{0.5}VO_4$ would take place due to large difference between La, Ce and Y as it happened to BYV solid solution. The minute quantity of gases produced by $La_{0.5}Y_{0.5}VO_4$ and $Ce_{0.5}Y_{0.5}VO_4$ indicated that distortion of VO_4 tetrahedron was not a key factor for zircon type V-based compounds alone. As a result, we suggested that both of Bi–O and V–O bond length should be responsible to the high activities of BMV solid solutions. The effect of Bi–O and V–O bond lengths on photocatalytic activities of samples should originate from its effect on electron structure, which we will discuss in the following section.

Table 4
Photocatalytic activities of $A_{0.5}Y_{0.5}VO_4$ (*A*=La, Ce, Bi) for water splitting under UV light.

Samples	Amounts of gas/μmol	
	H_2	O_2
$Bi_{0.5}Y_{0.5}VO_4$	901.6	414.4
$La_{0.5}Y_{0.5}VO_4$	0.2	0
$Ce_{0.5}Y_{0.5}VO_4$	0.5	0

3.5. Calculation of band structure and explanation for water splitting activity of BYV

To clarify band structure of BYV, we used the WIEN2k program with full-potential linearized augmented plane-wave method to calculate total and partial DOS of BYV as well as YVO_4 and $BiVO_4$ for comparison. YVO_4 and $BiVO_4$ possessed that band gap of direct transition due to the same *k* point. From the total DOS, band gaps of zircon-type $BiVO_4$ and YVO_4 were estimated to be 2.8 and 3.0 eV, respectively, consistent with report of Dolgos [36]. However, two types of transition in BYV solid solution are observed in Fig. 6. The smallest gap from P point to Γ point belonged to indirect transition and corresponded to energy level band. The direct transition locating at P point was 2.9 eV and considered as band gap of BYV. Band gap width of BYV locating between $BiVO_4$ and YVO_4 proved incorporation of Y into $BiVO_4$ increased band gap of $BiVO_4$ which is consistent with the results from DRS measurement mentioned above. As we knew, band gap refers to the energy difference between CBM and valence band maximum (VBM) in insulators and semiconductors. Decreased band gaps of BYV solid solution reflected some change should happen to the conduction band and valence band with Bi incorporation. In the following section, we will discuss about features of conduction band and valence band of BYV(0.5) and then compared them with those of isotopic $BiVO_4$. First, let us have a glance on panorama of partial DOSs of each element. O2*p* has a major contribution to VBM spreading between 0 and −5 eV. A small amount of O2*p* density was also observed in the CBM from 2.85 to 6 eV. V3*d* orbital also have contributions to both CBM and VBM. However, contribution of V3*d* to the VBM is rather smaller than that to CBM because of its high oxidation state and formal d^0 configuration. Bi6*s* contribution is largely confined to the bands from −8 to −10 eV. In addition, we can clearly see that some part of Bi6*s* orbitals also contributed to the top of valence band from −2 to 0 eV. As respect to Y cation, main contribution originated from Y4*d* not Y5*s*. pDOS of Y4*d* pervaded in the higher energy bands from 6 to 10 eV and left a rather small part in lower conduction band.

To have a deeper inspection on VBM and CBM of BYV, the contributions of each element around VBM (−0.7 to 0 eV) and CBM (2.86–3.6 eV) in BYV were calculated and are shown in Table 5 with the data of zircon-type $BiVO_4$. In the VBM of BYV solid solution, O2*p*, Bi6*s* and V3*d* orbitals occupied 90%, 8% and 2%, respectively; Y has no contribution. These data demonstrated that interaction of O2*p* and Bi6*s* should have an important role in the properties of VBM. Recently, Stoltzfus et al. proved Bi6*s* and O2*p* orbitals had an antibonding interaction at the top of the O2*p* valence band, namely the top of valence band of monoclinic type

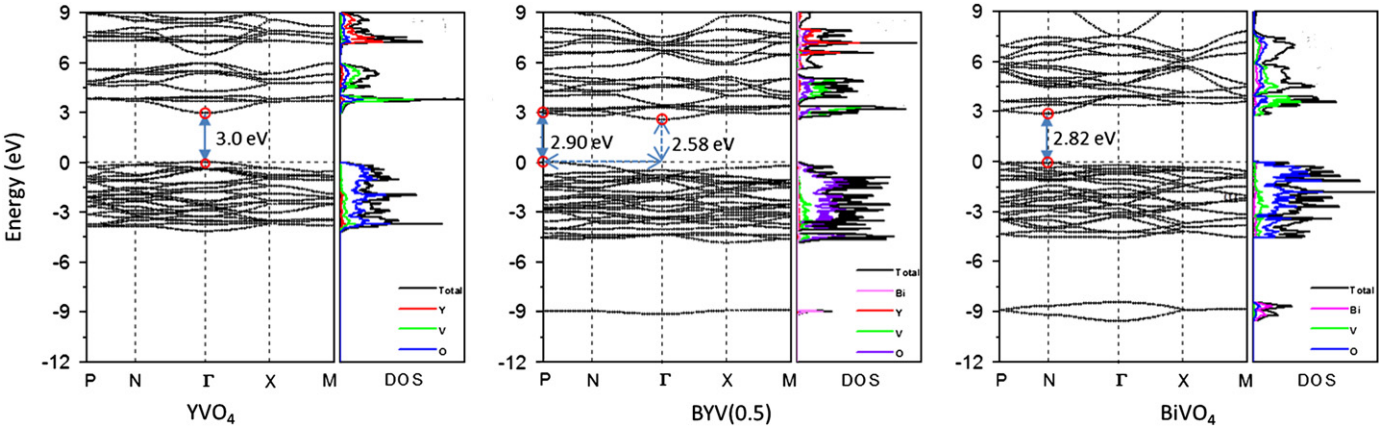

Fig. 6. DOS plots of zircon $BiVO_4$, YVO_4 and BYV solid solution.

Table 5
Contribution of each element to conduction band minimum and valence band maximum in BYV and $BiVO_4$.

Energy bands	BYV				$BiVO_4$			
	Bi	Y 4*d*	V 3*d*	O 2*p*	Bi	Y 4*d*	V 3*d*	O 2*p*
2.80 to 3.60 eV	5.7% (Bi 6*p*)	1.2%	71.5%	21.6%	8.9% (Bi 6*p*)	/	75.1%	16.0%
−0.7 to 0 eV	7.8% (Bi 6*s*)	0%	2.0%	90.1%	6.6% (Bi 6*s*)	/	2.6%	90.8%

$BiVO_4$, using cooperative overlap Hamiltonian population calculation [36]. This antibonding interaction of Bi6*s* lone pairs and O2*p* state in monoclinic $BiVO_4$ can produce lighter holes and electrons comparing to other metal oxides [36,37]. Such lighter holes and electrons are easy to migrate in the energy band of semiconductors, which facilitate separation of excited charges and increase the surface reaction with water. Although monoclinic $BiVO_4$ and zircon $BiVO_4$ have different crystal structures, we believed this mechanism also will happen to zircon $BiVO_4$ because both of them have the antibonding interactions between Bi6*s* and O2*p*. As a derivative of zircon $BiVO_4$, BYV has same crystal structure and similar VBM constituent shown in Table 4 because Y4*d* has no contribution to VBM. Therefore we deduce that photoexcited carriers should own the relative lighter effective masses that it seems to carry in the semiclassical model of transport in a crystal due to the antibonding interaction of Bi6*s* and O2*p* and then lead to highly efficient overall water splitting of BMV solid solutions.

When turning to CBM (2.85–3.60 eV), Bi6*p* and Y4*d* gave a small contribution around 6% and 1%, respectively. The left part of CBM came from V3*d* (71%) and O2*p* (22%). However, in zircon-type $BiVO_4$, the contribution of Bi6*p* and V3*d* in 2.80–3.60 eV increased to 8.9% and 75.1%, respectively; O2*p* decreased to 16.0%. Although Y cation was proved to play an important role in determining H_2 producing activity of BYV in the photocatalytic experiments, the calculation of BYV solid solution indicated that Y cation has little direct effect on band structure due to the 1% contribution from Y4*d* orbital. This conclusion was consistent with discussion in DRS measurement. Therefore, weakened interaction of Bi6*p* and VO_4 tetrahedron by replacing Bi with *M* cations was the key reason for the H_2 production of BMV solid solution.

4. Conclusions

$Bi_{0.5}M_{0.5}VO_4$ (*M*=La, Eu, Sm and Y) solid solutions were synthesized using the solid state reaction. Bi6*s* lone pair was proved to exist in constrained state in B*M*V solid solution of zircon type structure by investigating the effective ionic radius of Bi cation. *M*–O bond lengths of B*M*V solid solutions were increased with effective ionic radii of *M* cations. All the samples have the ability to split water to H_2 and O_2 at the same time under UV light irradiation, which was improved in the decreasing order of *M* cations. Incorporation of Bi rather than distortion of VO_4 tetrahedron were the key factor for highly efficient activity. Incorporation of *M* cations has no direct contribution to conduction band minimum, but gave indirect contribution by weakening interaction between Bi and VO_4 tetrahedron by substituting Bi. From the calculation, interaction of Bi6*s* and O2*p* was considered as a reason for the effective overall water splitting of B*M*V solid solutions by facilitating the generation of electron and hole with lighter effective masses.

Acknowledgments

Authors acknowledge the support from the National Key Basic Research and Development Program (Nos. 2003CB214500, 2009CB220000), the National Natural Science Foundation of China (No. 20973110), and from a grant from the Global-Centre of Excellence in Novel Carbon Resource Sciences, Kyushu University, Japan.

References

[1] A. Fujishima, K. Honda, Nature 238 (5358) (1972) 37–38.
[2] M. Kitano, M. Hara, J. Mater. Chem. 20 (4) (2010) 627–641.
[3] A. Kudo, H. Kato, I. Tsuji, Chem. Lett. 33 (12) (2004) 1534–1539.
[4] X. Chen, S. Shen, L. Guo, S.S. Mao, Chem. Rev. 110 (11) (2010) 6503–6570.
[5] M. Matsuoka, M. Kitano, M. Takeuchi, K. Tsujimaru, M. Anpo, J.M. Thomas, Catal. Today 122 (1-2) (2007) 51–61.
[6] A.J. Bard, M.A. Fox, Acc. Chem. Res. 28 (3) (1995) 141–145.
[7] H. Liu, J. Yuan, W. Shangguan, Energy Fuels 20 (6) (2006) 2289–2292.
[8] A.L. Linsebigler, G. Lu, J.T. Yates, Chem. Rev. 95 (3) (1995) 735–758.
[9] A. Kudo, K. Omori, H. Kato, J. Am. Chem. Soc. 121 (49) (1999) 11459–11467.
[10] H. Kato, A. Kudo, J. Phys. Chem. B 105 (19) (2001) 4285–4292.
[11] M. Machida, J.-I. Yabunaka, T. Kijima, S. Matsushima, M. Arai, Int. J Inorg. Mater. 3 (6) (2001) 545–550.
[12] K. Sayama, S. Tsukagoshi, T. Mori, K. Hara, Y. Ohga, A. Shinpou, Y. Abe, S. Suga, H. Arakawa, Sol. Energy Mater. Sol. Cells 80 (1) (2003) 47–71.
[13] Y. Tachibana, K. Hara, K. Sayama, H. Arakawa, Chem. Mater. 14 (6) (2002) 2527–2535.
[14] T. Thompson, J. Yates, Top. Catal. 35 (3) (2005) 197–210.
[15] A. Kudo, H. Kato, Chem. Phys. Lett. 331 (5-6) (2000) 373–377.
[16] A. Iwase, H. Kato, H. Okutomi, A. Kudo, Chem. Lett. 33 (10) (2004) 1260–1261.
[17] A. Kudo, Y. Miseki, Chem. Soc. Rev. 38 (1) (2009) 253–278.
[18] K. Domen, S. Naito, T. Onishi, K. Tamaru, Chem. Phys. Lett. 92 (4) (1982) 433–434.
[19] K. Sayama, H. Arakawa, J. Photochem. Photobiol. A 77 (2-3) (1994) 243–247.
[20] M. Hara, H. Hasei, M. Yashima, S. Ikeda, T. Takata, J.N. Kondo, K. Domen, Appl. Catal. A 190 (1–2) (2000) 35–42.
[21] H. Liu, J. Yuan, Z. Jiang, W. Shangguan, H. Einaga, Y. Teraoka, J. Mater. Chem. 21 (41) (2011) 16535–16543.
[22] A. Watanabe, J. Solid State Chem. 153 (1) (2000) 174–179.
[23] K. Maeda, K. Teramura, N. Saito, Y. Inoue, K. Domen, J. Catal. 243 (2) (2006) 303–308.
[24] K. Maeda, K. Teramura, D.L. Lu, T. Takata, N. Saito, Y. Inoue, K. Domen, Nature 440 (7082) (2006) 295.
[25] J. Rodríguez-Carvajal, Physica B 192 (1–2) (1993) 55–69.
[26] J.P. Perdew, K. Burke, M. Ernzerhof, Phys. Rev. Lett. 77 (18) (1996) 3865.
[27] P.E. Blochl, O. Jepsen, O.K. Andersen, Phys. Rev. B 49 (23) (1994) 16223.
[28] R. Shannon, Acta Cryst. A 32 (5) (1976) 751–767.
[29] F.D. Hardcastle, I.E. Wachs, J. Phys. Chem. 95 (13) (1991) 5031–5041.
[30] M. Liegeois-Duyckaerts, P. Tarte, Spectrochim. Acta A 28 (11) (1972) 2037–2051.
[31] M. Machida, J. Yabunaka, T. Kijima, Chem. Mater. 12 (3) (2000) 812–817.
[32] A. Kudo, H. Okutomi, H. Kato, Chem. Lett. 10 (2000) 1212–1213.
[33] Z. Zou, J. Ye, H. Arakawa, J. Phys. Chem. B 106 (3) (2002) 517–520.
[34] M.R. Dolgos, A.M. Paraskos, M.W. Stoltzfus, S.C. Yarnell, P.M. Woodward, J. Solid State Chem. 182 (7) (2009) 1964–1971.
[35] A.C. Stuckl, C.A. Daul, H.U. Gudel, J. Chem. Phys. 107 (12) (1997) 4606–4617.
[36] M.W. Stoltzfus, P.M. Woodward, R. Seshadri, J.-H. Klepeis, B. Bursten, Inorg. Chem. 46 (10) (2007) 3839–3850.
[37] A. Walsh, Y. Yan, M.N. Huda, M.M. Al-Jassim, S.-H. Wei, Chem. Mater. 21 (3) (2009) 547–551.
[38] S. Murugesan, M.N. Huda, Y. Yan, M.M. Al-Jassim, V. Subramanian, J. Phys. Chem. C 114 (23) (2010) 10598–10605.
[39] J. Yu, A. Kudo, Adv. Funct. Mater. 16 (16) (2006) 2163–2169.
[40] H. Duclusaud, S.A. Borshch, Chem. Phys. Lett. 290 (4–6) (1998) 526–534.
[41] K. Maeda, K. Teramura, D.L. Lu, T. Takata, N. Saito, Y. Inoue, K. Domen, J. Phys. Chem. B 110 (28) (2006) 13753–13758.